Intrinsic anisotropic magnetic, electrical, and thermal transport properties of *d*-Al-Co-Ni decagonal quasicrystals

M. Bobnar,[1] P. Jeglič,[1,2] M. Klanjšek,[1,2] Z. Jagličić,[3] M. Wencka,[4] P. Popčević,[5] J. Ivkov,[5] D. Stanić,[5] A. Smontara,[5] P. Gille,[6] and J. Dolinšek[1,2,*]

[1]*Jozef Stefan Institute & University of Ljubljana, Faculty of Mathematics and Physics, Jamova 39, SI-1000 Ljubljana, Slovenia*

[2]*EN-FIST Centre of Excellence, Dunajska 156, SI-1000 Ljubljana, Slovenia*

[3]*Institute of Mathematics, Physics and Mechanics & University of Ljubljana, Faculty of Civil and Geodetic Engineering, Jamova 2, SI-1000 Ljubljana, Slovenia*

[4]*Institute of Molecular Physics, Polish Academy of Sciences, Smoluchowskiego 17, 60-179 Poznań, Poland*

[5]*Institute of Physics, Laboratory for the Study of Transport Problems, Bijenička 46, POB 304, HR-10001 Zagreb, Croatia*

[6]*Ludwig-Maximilians-Universität München, Department of Earth and Environmental Sciences, Crystallography Section, Theresienstrasse 41, D-80333 München, Germany*

(Received 4 October 2011; revised manuscript received 26 November 2011; published 20 January 2012)

To address the questions on the anisotropy of bulk physical properties of decagonal quasicrystals and the intrinsic physical properties of the *d*-Al-Co-Ni phase, we investigated the anisotropic magnetic susceptibility, the electrical resistivity, the thermoelectric power, the Hall coefficient, and the thermal conductivity of a *d*-Al-Co-Ni single crystal of exceptional structural quality. Superior structural order on the local scale of atomic clusters was confirmed by ^{27}Al nuclear magnetic resonance spectroscopy. The measurements were performed in the 10-fold periodic direction of the structure and in three specific crystallographic directions within the quasiperiodic plane, corresponding to the 2 and 2′ twofold symmetry directions and their bisector. The specific heat, being a scalar quantity, was determined as well. The measurements of the second-rank bulk tensorial properties confirm the theoretical prediction that a solid of decagonal point group symmetry should exhibit isotropic physical properties within the quasiperiodic plane and anisotropy between the in-plane and the 10-fold directions. *d*-Al-Co-Ni is an anisotropic diamagnet with stronger diamagnetism for the magnetic field in the 10-fold direction. Electrical and thermal transport is strongly metallic in the 10-fold direction but largely suppressed within the quasiperiodic plane, the main reason being the lack of translational periodicity that hinders the propagation of electrons and phonons in a nonperiodic lattice. The third-rank Hall-coefficient tensor shows sign-reversal anisotropy related to the direction of the magnetic field when applied in the 10-fold direction or within the quasiperiodic plane. The observed anisotropy is not a peculiarity of quasicrystals but should be a general feature of solids with broken translational periodicity in two dimensions.

DOI: 10.1103/PhysRevB.85.024205 PACS number(s): 61.44.Br, 71.23.Ft, 76.60.−k

I. INTRODUCTION

One of the basic open questions in the physics of quasicrystals (QCs) is whether the quasiperiodicity of the structure influences the physical properties of a solid in a fundamental way by introducing qualitatively new phenomena or whether the unusual properties are a consequence of complex local atomic order with no direct relationship to the quasiperiodicity. To elucidate this question, decagonal quasicrystals (*d*-QCs) are of particular importance because their structure can be viewed as a periodic stacking of quasiperiodic atomic planes. Thus, *d*-QCs are two-dimensional QCs, whereas they are periodic crystals in a direction perpendicular to the quasiperiodic planes. Consequently, the physical properties of the *d*-QCs can be studied in the quasiperiodic (Q) and periodic (10-fold) crystallographic directions on the same sample. Structural anisotropy of *d*-QCs results in their anisotropic magnetic, electrical, and thermal transport properties.

The most studied *d*-QCs are those from the ternary Al-Co-Ni and Al-Co-Cu systems, which form thermodynamically stable phases and for which conventional crystal growth techniques can be used to grow large single crystals.[1,2] At a qualitative level, their anisotropic physical properties (the magnetic susceptibility, the electrical resistivity, the thermoelectric power, the Hall coefficient, and the thermal conductivity) show some common behavior, like the anisotropy of electrical resistivity between the Q and the 10-fold directions in the range $\rho_Q/\rho_{10} = 4$–10[3–7] and the crystallographic-direction-dependent sign of the Hall coefficient, being electronlike ($R_H < 0$) for the magnetic field application in the 10-fold direction and holelike ($R_H > 0$) for the Q (in-plane) direction.[8] However, important quantitative differences were found for samples of nominally the same or slightly different chemical compositions and perhaps structural qualities. A striking example is electrical resistivity, for which some studies[3,4] report that both ρ_{10} and ρ_Q exhibit a metallic positive temperature coefficient (PTC), whereas other studies[5–7] report that only ρ_{10} is metallic, whereas ρ_Q exhibits a nonmetallic negative temperature coefficient (NTC). The nonmetallic behavior of ρ_Q was suggested to originate from the phonon-assisted tunneling of charge carriers in extended states[5] or from an enhanced electron–phonon and phonon–phonon coupling in the quasiperiodic plane.[6] Because phonons cannot propagate easily in a quasiperiodic structure that lacks translational periodicity, the preceding hypotheses deserve further consideration. The anisotropic magnetism of *d*-QCs brings up another controversy. Markert *et al.*[4] reported that *d*-$Al_{70}Co_{15}Ni_{15}$ is a Curie paramagnet for the magnetic field application in both the

10-fold and the Q directions with 10% anisotropy in magnetic susceptibility and containing a weak ferromagnetic (FM) component. In contrast, Yamada *et al.*[8] reported qualitatively different behavior, in which magnetization as a function of the magnetic field initially increased with an increasing field up to the maximum at about 5 kOe, whereas for higher fields it decreased linearly and the negative slope was larger for the field application in the 10-fold direction. The authors concluded that *d*-Al-Co-Ni is an anisotropic diamagnet, which is more diamagnetic for the field application in the 10-fold direction, whereas the maximum in $M(H)$ originates from a small FM spin fraction present in the samples.

In all preceding studies, the Q direction was not specified in more detail, lying somewhere arbitrarily in the quasiperiodic plane. Because the quasiperiodic plane of the *d*-Al-Co-Ni(Cu) structure contains 20 twofold directions,[9] it is desirable to perform measurements within this plane in a more controlled manner in well-defined crystallographic directions. Moreover, frequent contradicting reports on the same physical property, when measured on samples with nominally the same or similar chemical compositions but with different structural perfections, also raise questions about the true intrinsic properties of the *d*-Al-Co-Ni phase. In this paper, we report on the anisotropic physical properties of a large *d*-Al-Co-Ni single crystal of exceptional structural quality, so we believe that we report on the true intrinsic properties of this phase. Using ^{27}Al nuclear magnetic resonance (NMR) spectroscopy, we first demonstrate superior structural order on the local scale of atomic clusters and then present the anisotropic magnetic, electrical, and thermal transport properties (the magnetic susceptibility, the electrical resistivity, the thermoelectric power, the Hall coefficient, and the thermal conductivity) measured in the 10-fold direction and three crystallographic directions within the quasiperiodic plane. The specific heat, being a scalar quantity, was determined as well. Performing analysis of the measurements in the 10-fold and Q directions, we address the question about the influence of quasiperiodicity on the physical properties of a solid. This work complements and rounds up our recent investigations of anisotropic physical properties of giant-unit-cell decagonal approximant phases that possess a stacked-layer structure but contain different numbers of atomic layers within one periodic unit in the stacking direction—the two-layer Y-phase Al-Co-Ni;[10,11] the four-layer compounds $Al_4(Cr,Fe)$,[12,13] $Al_{13}Co_4$,[14] $Al_{13}Fe_4$, and $Al_{13}(Fe,Ni)_4$[15]; and the six-layer Taylor phase $Al_3(Mn,Fe)$[16]—as compared to the two-layer *d*-Al-Co-Ni QC.

II. STRUCTURAL CONSIDERATIONS AND SAMPLE PREPARATION

The quasiperiodic plane of the *d*-Al-Co-Ni structure is perpendicular to the [00001] 10-fold direction and contains 20 directions (including the opposite ones) that correspond to the positions of 10 twofold axes.[9] These twofold axes belong to two sets, sometimes called 2 and 2′ (denoted crystallographically as sets $\langle 10000\rangle$ and $\langle 10\bar{1}00\rangle$, respectively), which are not equivalent to each other but rather are rotated by 18° with respect to the other set. The angle between two neighboring twofold directions of a given set amounts to 36°. The quasiperiodic plane with the 20 twofold directions is shown in Fig. 1(a), where the directions of set 2 are given by solid lines and those of set 2′ by dashed lines. The particular directions [01000] of set 2 and [$10\bar{1}00$] of set 2′, which are perpendicular to each other, are shown in bold. An idealized polyhedron of the *d*-Al-Co-Ni QC of point group 10/*mmm*, using the concept of net planes[17] (being analogous to lattice planes for periodic crystals), is shown in Fig. 1(b). Each of the 20 side facets of the polyhedron is normal to one of the twofold directions shown in Fig. 1(a).

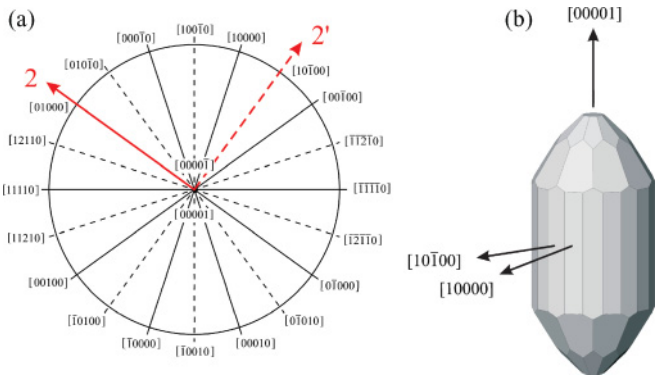

FIG. 1. (Color online) (a) The quasiperiodic plane of the *d*-Al-Co-Ni structure with the 20 twofold directions, where the directions of set 2 are given by solid lines and those of set 2′ by dashed lines. The particular directions [01000] of set 2 and [$10\bar{1}00$] of set 2′, which are orthogonal to each other and were employed as the measurement directions, are shown in bold. (b) An idealized polyhedron of the *d*-Al-Co-Ni QC of point group 10/*mmm*, using the concept of net planes (Ref. 17). Each of the 20 side facets of the polyhedron is normal to one of the twofold directions shown in panel (a).

Our centimeter-size single crystal was grown by the Czochralski method. Electron probe microanalysis (EPMA) measurements yielded the average composition of $Al_{69.7}Co_{10.0}Ni_{20.3}$ with a standard deviation of 0.2 at.% for each component. This composition is close to the Ni-rich limit of the QC stability region. Details of the sample preparation and characterization by x-ray transmission topography and other techniques are published elsewhere,[18] demonstrating the high structural quality of the material. The radial elemental distribution was found to be absolutely homogeneous within the error of EPMA. The crystal exhibited facets on as-grown surfaces, corresponding to those of the polyhedron shown in Fig. 1(b).

To perform crystallographic-direction-dependent measurements, we cut from the parent crystal four rectangular bars of the dimensions $10 \times 2 \times 2$ mm^3. Three of the bars had the edges of the parallelepipeds directed in three orthogonal crystallographic directions, the [00001] 10-fold direction, the [01000] 2 direction, and the [$10\bar{1}00$] 2′ direction (the last two are shown in bold in Fig. 1(a)), where each bar had its long axis in a different direction of this set. The fourth bar was cut with its long axis in the in-plane direction [$20\bar{1}00$] that is a bisector of two neighboring 2 and 2′ directions, lying at an angle of 9° to each of the former ones (in the following text, this direction is referred to as the *bis* direction), whereas the other two edges were in the [00001] 10-fold direction and the [13110] in-plane direction. A sketch of the crystallographic directions of the four bars is shown in Fig. 2(a). Our samples were thus oriented with

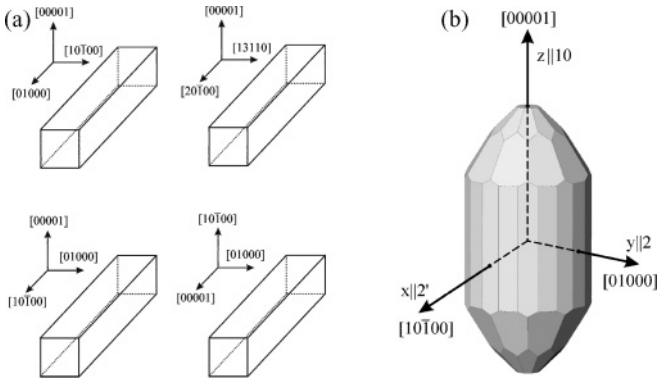

FIG. 2. (a) The crystallographic directions of the four bar-shaped d-Al-Co-Ni samples used in the measurements of the anisotropic physical properties. Here, [00001] is a 10-fold direction, [01000] is a 2 twofold direction, [10$\bar{1}$00] is a 2′ twofold direction, [20$\bar{1}$00] is a bisector of two neighboring 2 and 2′ directions lying at an angle of 9° to each of them (denoted as the *bis* direction), and [13110] is an in-plane direction perpendicular to the 10-fold and the *bis* directions. (b) The choice of axes of a Cartesian x,y,z crystal-fixed coordinate system for symmetry analysis of a general second-rank tensor of decagonal point group 10/*mmm* symmetry.

their long axes in the 10-fold direction and three directions in the quasiperiodic plane, the 2, the 2′, and the *bis* directions; the orientations of the other two orthogonal directions were known for each sample as well. The thus-prepared samples enabled us to determine the physical properties of the d-Al-Co-Ni QC in well-defined directions of the decagonal symmetry group.

III. SYMMETRY ANALYSIS OF THE BULK TENSORIAL PHYSICAL PROPERTIES

In an anisotropic crystal, bulk physical properties like the magnetic susceptibility χ, the electrical conductivity σ (the inverse resistivity $\sigma = \rho^{-1}$), the thermoelectric power S, and the thermal conductivity κ are symmetric (and diagonalizable) second-rank tensors. For example, the electrical conductivity tensor σ_{ij} relates the current density $\vec{j}$ to the electrical field $\vec{E}$ via the relation $j_i = \sum_j \sigma_{ij} E_j$, where $i,j = x,y,z$ denote crystallographic directions in a Cartesian coordinate system. The Hall coefficient $R_H^{ijk} = E_j/j_i B_k$ is a third-rank tensor, with i,j,k denoting crystallographic directions of the current j_i, the Hall electrical field E_j, and the magnetic field B_k. The tensorial ellipsoids exhibit the same symmetry axes as the crystallographic structure. The invariance of the tensors on the symmetry operations of a given point group determines the form of the tensors. Using the decagonal point group symmetry, we determine the general form of a second-rank tensor of a d-QC.

Because the [00001] 10-fold, the [01000] 2, and the [10$\bar{1}$00] 2′ crystallographic directions are mutually perpendicular, they represent a convenient choice for the axes of a Cartesian x,y,z crystal-fixed coordinate system. We assume that $x \| 2'$, $y \| 2$, and $z \| 10$ in the preceding set of directions [Fig. 2(b)]. Because of the twofold axes in the x and y directions, the T_{xz} and T_{yz} off-diagonal elements of an arbitrary symmetric second-rank tensor T_{ij} are zero by symmetry. The 10-fold axis in the z direction causes the T_{xy} off-diagonal element to vanish and the T_{xx} and T_{yy} diagonal elements to be equal. A second-rank tensor T_{ij} of decagonal symmetry is thus diagonal in the preceding Cartesian system with the general form

$$T_{ij} = \begin{vmatrix} a & 0 & 0 \\ 0 & a & 0 \\ 0 & 0 & b \end{vmatrix}. \quad (1)$$

Therefore, the material of ideal decagonal symmetry should be isotropic in the quasiperiodic plane regarding the bulk physical properties but should show anisotropy between the quasiperiodic plane and the periodic 10-fold direction.

IV. LOCAL-SCALE SYMMETRY ANALYSIS BY ^{27}Al NMR

While x-ray crystallography is an indispensable tool for the structure determination of QCs, it yields an average structure over the crystal and cannot give local details such as local deviations from the average structure. NMR spectroscopy offers complementary structural information on the local atomic scale of several interatomic distances. Orientation-dependent NMR spectra of quadrupolar nuclei such as ^{27}Al in a magnetic field provide information on (1) the distribution of electrical field gradient (EFG) and the magnetic-shielding tensors and the associated distribution of local atomic environments around the resonant nuclei, (2) the number of crystallographically inequivalent lattice sites, (3) the local symmetry of the crystalline lattice, and (4) the configurational disorder of a particular atomic cluster in the structure. ^{27}Al NMR is thus suitable to assess the structural quality of our d-Al-Co-Ni samples on the scale of atomic clusters. The details of the method to determine the symmetry of local chemical environments in Al-containing complex intermetallics were published elsewhere.[19,20] The method is based on the measurement of rotation patterns of ^{27}Al NMR spectra for rotations about particular symmetry directions of the crystallographic structure. The orientation-dependent intensity of absorption in a given frequency window on the satellite part of the ^{27}Al spectrum then shows the same symmetry as the local chemical environments around the ^{27}Al resonant nuclei within a spherical-like volume of diameter of several interatomic distances. The local character of the information originates from the EFG at the ^{27}Al sites being produced predominantly by the electrical charges from the near-neighbor atomic coordination shells and the EFG falling off with the distance from the electrical charge as $1/r^3$.

Our ^{27}Al NMR experiments were conducted in a magnetic field $B_0 = 9.39$ T at the temperature $T = 80$ K. The broad absorption spectra extend over the frequency interval of 5 MHz and were recorded by a frequency-sweep technique. The shape of the strongly inhomogeneously broadened ^{27}Al NMR spectrum of d-Al-Co-Ni is predominantly determined by the electrical quadrupole interaction.[20] A ^{27}Al (spin $I = 5/2$) spectrum of our $Al_{69.7}Co_{10.0}Ni_{20.3}$ for the magnetic field parallel to a 2′ twofold direction ($B_0 \| 2'$) is shown in Fig. 3. The spectrum shows the structure of a broad, low-intensity "background" line, corresponding to the first-order quadrupole-perturbed $\pm 5/2 \leftrightarrow \pm 3/2$ and $\pm 3/2 \leftrightarrow \pm 1/2$ satellite transitions and a narrow, high-intensity central line

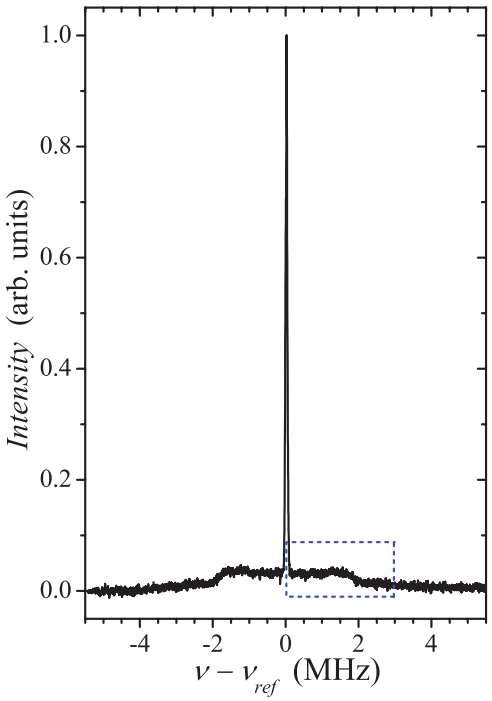

FIG. 3. (Color online) The ^{27}Al frequency-swept NMR spectrum of d-Al-Co-Ni in a magnetic field $B_0 = 9.39$ T at the temperature $T = 80$ K for the field parallel to a 2′ twofold direction ($B_0 \| 2'$). The reference frequency on the horizontal scale corresponds to the ^{27}Al Larmor frequency $\nu_{\mathrm{ref}} = 104.101$ MHz. The dashed box encloses part of the satellite spectrum used to determine the intensity variation upon rotating the crystal (see the text).

$(1/2 \leftrightarrow -1/2$ transition) in the middle of the spectrum that is quadrupole perturbed in the second order. By rotating the samples in the magnetic field, the position and shape of the central line did not change considerably, whereas significant intensity variations were observed on the satellite part of the spectrum.

To record the rotation patterns of the intensity variation over the spectrum, the samples were rotated about an axis perpendicular to the magnetic field. The rotation axis was chosen to coincide with the 10-fold, 2, and 2′ directions. In Fig. 4(a), part of the satellite spectrum (the part that is enclosed in a dashed box in Fig. 3) for the rotation about the 2 twofold direction is shown on an expanded scale for three particular angles, $\alpha = 0°$, 45°, and 90°, between the 10-fold axis and the magnetic field. The orientation-dependent intensity variation in the interval $\alpha = [0°, 180°]$ recorded at the frequency ν_1 (marked by a dashed arrow in Fig. 4(a)), is shown in Fig. 4(b). The pattern shows the symmetry of a twofold axis, where the angle $\alpha = 90°$ represents a plane of mirror symmetry. A twofold symmetric pattern is also obtained for rotation about the 2′ direction, as shown in Figs. 4(c) and 4(d). The orientation-dependent spectra and the intensity patterns for rotation about the 10-fold direction are shown in Figs. 5(a)–5(c), where α now denotes the angle between the 2 twofold axis and the magnetic field. The intensity patterns were recorded at two frequencies, ν_1 and ν_2 [marked by dashed arrows in Fig. 5(a)], and are displayed in the interval $\alpha = [0°, 36°]$ in Figs. 5(b) and 5(c). The patterns repeat themselves

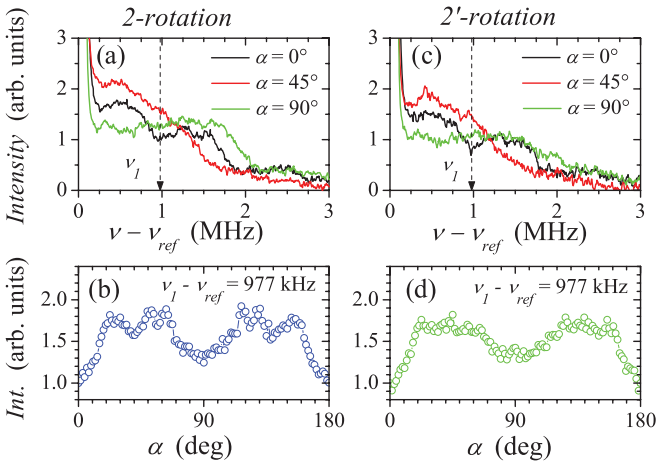

FIG. 4. (Color online) (a) An expanded part of the ^{27}Al NMR satellite spectrum (the part enclosed in a dashed box in Fig. 3) for rotation about the 2 twofold direction for three particular angles, $\alpha = 0°$, 45°, and 90°, between the 10-fold axis and the magnetic field. (b) The orientation-dependent intensity variation in the interval $\alpha = [0°, 180°]$ recorded at the frequency ν_1 (marked by a dashed arrow in panel (a)). (c) and (d) The corresponding spectrum and the intensity variation for the rotation about the 2′ twofold direction.

exactly after 36°, consistent with the 10-fold symmetry of the structure. The patterns repeat approximately, but not exactly, after 18° [the minimum at 18° in Fig. 5(b) is deeper than the minima at 0° and 36°, whereas in Fig. 5(c) the maximum at 18° has a different shape than the maxima at 0° and 36°]. The angle $\alpha = 0°$ corresponds to the orientation $B_0 \| 2$ and $\alpha = 18°$ corresponds to $B_0 \| 2'$, which confirms the nonequivalence of the 2 and 2′ sets of twofold axes. The angle $\alpha = 9°$ corresponds to the orientation at which a bisector of the 2 and 2′ directions, i.e., the in-plane *bis* direction $[20\bar{1}00]$, is parallel to the magnetic field. The repetition of the intensity patterns after 36°

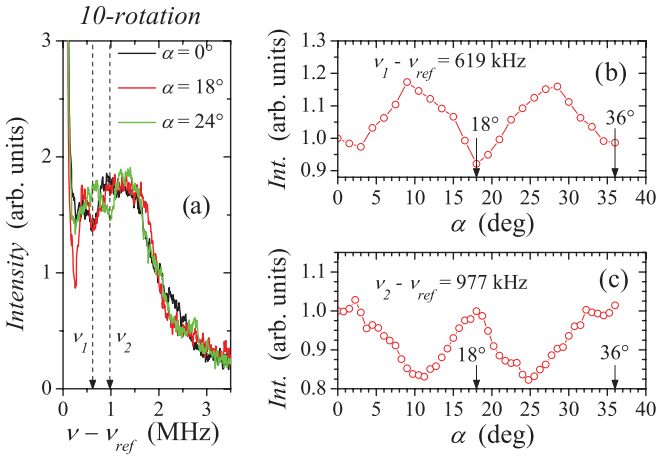

FIG. 5. (Color online) (a) An expanded part of the ^{27}Al NMR satellite spectrum (the part enclosed in a dashed box in Fig. 3) for rotation about the 10-fold direction for three particular angles, $\alpha = 0°$, 18°, and 24°, between the 2 twofold axis and the magnetic field. (b) and (c) The orientation-dependent intensity variation in the interval $\alpha = [0°, 36°]$ recorded at the frequencies ν_1 and ν_2 (marked by dashed arrows in panel (a)).

thus clearly demonstrates the crystallographic inequivalence of the 2, 2′, and *bis* directions.

The ^{27}Al NMR-intensity rotation patterns of Figs. 4 and 5 demonstrate well-developed symmetries of local chemical environments in our *d*-Al-Co-Ni material that are consistent with the elements of the decagonal point group. The macroscopic average decagonal symmetry, as determined by x-rays, is thus preserved on the local scale of atomic clusters as well, confirming that our quasicrystalline material is locally well ordered.

V. EXPERIMENTAL RESULTS

Magnetic measurements were conducted by a Quantum Design MPMS XL-5 superconducting quantum interference device magnetometer equipped with a 50-kOe magnet, operating in the temperature range 1.9–400 K. The measurements of the electrical resistivity, the thermoelectric power, the Hall coefficient, the thermal conductivity, and the specific heat were conducted by a Quantum Design physical property measurement system (PPMS 9T) equipped with a 90-kOe magnet and operating in the temperature range 2–400 K. Electrical resistivity was measured by a standard four-terminal technique. The thermoelectric power and the thermal conductivity were measured simultaneously by monitoring both the temperature and the voltage drop across the sample as a square-wave heat pulse is applied to one of its ends. The Hall-coefficient measurements were performed by the five-point method using the standard alternating current technique in magnetic fields up to 10 kOe. Specific heat was measured by a thermal-relaxation calorimeter.

A. Magnetization and magnetic susceptibility

In the first set of measurements, the magnetization versus the magnetic field curves $M(H)$ were determined at $T = 5$ K for the magnetic field sweep of ±50 kOe applied in the 10, 2, 2′, and *bis* crystallographic directions [Fig. 6(a)]. All curves show linear, negative-slope, diamagnetic behavior. While there is no anisotropy among the three in-plane directions (2, 2′, and *bis*), anisotropy exists to the 10-fold direction, which has a larger negative slope, i.e., the material is more diamagnetic in this direction.

The magnetic susceptibility $\chi = M/H$, determined in the temperature range 1.9–300 K in the magnetic field $H =$ 1 kOe applied in the 10, 2, 2′, and *bis* directions, is shown in Fig. 6(b). The results are consistent with the $M(H)$ curves of Fig. 6(a), with all susceptibilities being negative diamagnetic. There is no anisotropy among the three in-plane directions, whereas anisotropy exists to the 10-fold direction, which is more diamagnetic. The zero-field-cooled and field-cooled susceptibilities show small splitting below 10 K, which can be attributed to a tiny FM component, likely of extrinsic origin, to the *d*-Al-Co-Ni phase (e.g., FM surface oxides and/or Co- or Ni-rich magnetic clusters in the vicinity of defects). The FM component is, however, very small, amounting to a small fraction of the diamagnetic susceptibility, and is much smaller than the FM fractions reported in other investigations of magnetic properties of *d*-Al-Co-Ni.[4,8]

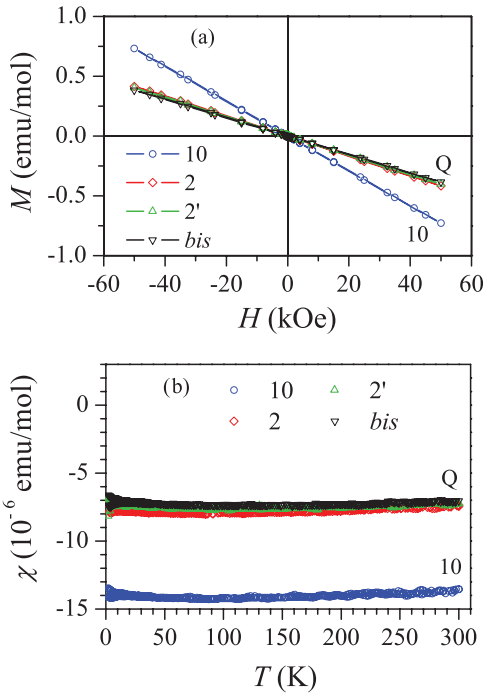

FIG. 6. (Color online) (a) The magnetization versus the magnetic field curves $M(H)$ of *d*-Al-Co-Ni determined at $T = 5$ K for the magnetic field sweep of ±50 kOe applied in the 10, 2, 2′, and *bis* crystallographic directions. (b) The magnetic susceptibility $\chi = M/H$ determined in the temperature range 1.9–300 K in the magnetic field $H = 1$ kOe. The index Q is conveniently used for the three investigated in-plane directions (2, 2′, and *bis*).

The Larmor diamagnetic susceptibility of closed atomic shells for the $Al_{69.7}Co_{10.0}Ni_{20.3}$ composition was calculated from literature tables[21] to amount to $\chi_{dia} = -5 \times 10^{-6}$ emu/mol, which is very close to the room-temperature (RT) values of the three isotropic in-plane susceptibilities shown in Fig. 6(b) (amounting to $\chi_2 \approx \chi_{2'} \approx \chi_{bis} = -7 \times 10^{-6}$ emu/mol). This demonstrates that the in-plane susceptibility can be practically fully accounted for by the Larmor diamagnetism. Because the contribution of the FM spin fraction to the susceptibility is a small fraction of $|\chi_{dia}|$, this also demonstrates that negligible fractions of Co and/or Ni spins are involved in the FM-ordered clusters. The susceptibility in the 10-fold direction is about two times more diamagnetic than the in-plane susceptibilities, with the RT value $\chi_{10} = -14 \times 10^{-6}$ emu/mol. This can be explained by an additional Landau diamagnetic contribution present for the field application in this crystallographic direction because of the conduction-electron orbital circulation in a plane perpendicular to the 10-fold direction, thus in the quasiperiodic plane. The Landau diamagnetic contribution to the susceptibility is theoretically of the same order of magnitude as that due to the Larmor diamagnetism. The presence of Landau diamagnetic contribution for the field application in the 10-fold direction and its absence for the in-plane application can be understood from the structural considerations of the *d*-Al-Co-Ni phase. According to the structural model by Burkov,[22] and observed experimentally,[23] the *d*-Al-Co-Ni structure can be viewed as a set of overlapping decagonal columnar clusters of a

10.3-Å radius with the long axis along the 10-fold axis, where decagonal atomic rings are located in the perpendicular quasiperiodic planes. These atomic rings represent circular electrical current loops when the magnetic field is applied in the 10-fold direction and provide Landau diamagnetic contribution to the magnetic susceptibility χ_{10}. Because the decagonal atomic rings and the associated circular current loops exist only in the quasiperiodic planes, no Landau diamagnetism is present for the magnetic field direction other than along the 10-fold axis, and χ_{10} is consequently more diamagnetic than the in-plane susceptibilities.

The *d*-Al-Co-Ni QC can thus be classified as an anisotropic diamagnet with no in-plane anisotropy and slight anisotropy to the 10-fold direction, where the magnetic anisotropy originates from the additional Landau orbital diamagnetic term present for the field application along the 10-fold axis due to the conduction-electron circulation within the decagonal atomic rings located in the quasiperiodic atomic planes. The diamagnetism of the *d*-Al-Co-Ni material also demonstrates that the transition metals Co and Ni are in a nonmagnetic state with their *d*-bands fully occupied (no unpaired *d*-type electrons are present).

B. Electrical resistivity

The electrical resistivity $\rho(T)$ data, measured between 340 and 2 K in the 10, 2, 2′, and *bis* directions, are shown in Fig. 7(a), whereas the resistivities normalized to their 340 K values, $\rho/\rho_{340\mathrm{K}}$, are shown in Fig. 7(b). The resistivities show no in-plane anisotropy, whereas there is considerable anisotropy between the in-plane direction and the 10-fold direction. At 340 K, $\rho_2 \approx \rho_{2'} \approx \rho_{\mathrm{bis}} = 303 \pm 4\ \mu\Omega$cm, where the scatter of the three in-plane resistivity values is by 3%, whereas $\rho_{10} = 36\ \mu\Omega$cm. This yields the anisotropy factor $\rho_Q/\rho_{10} = 8.4$ (where the index Q is conveniently used for all three in-plane directions). The 3% scatter in the absolute values of the in-plane resistivities is within the experimental error due to uncertainty in the determination of the samples' geometrical parameters (the length and the cross section). This is confirmed because the normalized in-plane resistivities in Fig. 7(b) perfectly overlap, demonstrating that they exhibit identical temperature dependence, and the tiny differences in their absolute values can be accounted for by constant scaling factors. The isotropy of the in-plane resistivity can thus be claimed unambiguously.

The resistivities exhibit metallic PTC for all four investigated directions. The PTC is large for the 10-fold direction, giving fractional increase between 2 and 340 K by $R_{10} = (\rho_{10}^{340\mathrm{K}} - \rho_{10}^{2\mathrm{K}})/\rho_{10}^{340\mathrm{K}} = 26\%$. For the three in-plane directions, the fractional increase is much smaller, amounting to $R_Q = (\rho_Q^{340\mathrm{K}} - \rho_Q^{2\mathrm{K}})/\rho_Q^{340\mathrm{K}} \approx 2\%$. Another marked difference between the in-plane and the periodic resistivities is their temperature dependence. While ρ_{10} exhibits linearlike increase upon heating at temperatures above the low-temperature saturated region, the in-plane resistivities show a tendency to exhibit maximum or at least leveling off at temperatures close to RT in their much weaker temperature dependence.

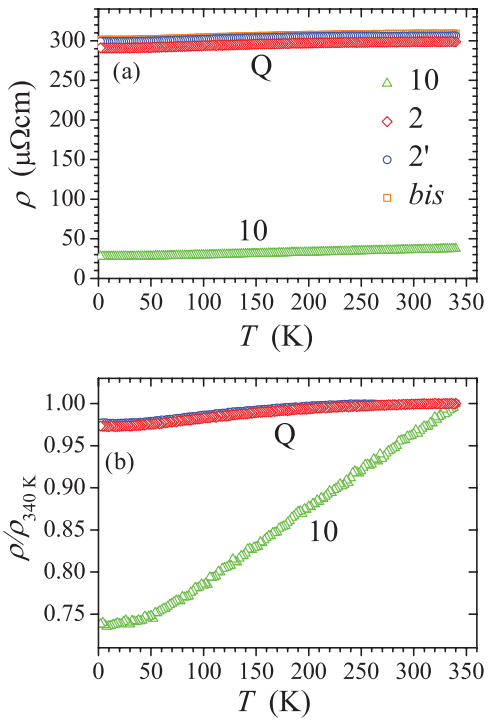

FIG. 7. (Color online) (a) Temperature-dependent electrical resistivity $\rho(T)$ measured in the 10, 2, 2′, and *bis* directions. (b) The resistivities normalized to their 340 K values, $\rho/\rho_{340\mathrm{K}}$. The index Q is conveniently used for the three investigated in-plane directions (2, 2′, and *bis*).

C. Thermoelectric power

The thermoelectric power data (the Seebeck coefficient *S*), measured between 310 and 2 K in the 10, 2, 2′, and *bis* directions are displayed in Fig. 8. There is again no anisotropy among the three in-plane directions, $S_2 = S_{2'} = S_{\mathrm{bis}}$, but there is significant anisotropy to S_{10} in the 10-fold direction. The thermopower values for all directions are small, up to a few microvolts per Kelvin at most and show rather complicated temperature dependence. S_{10} is negative in the low-temperature region but exhibits a minimum at 60 K with the value $-4\ \mu$V/K where its slope is reversed so that S_{10} changes sign to positive at 250 K. The three in-plane

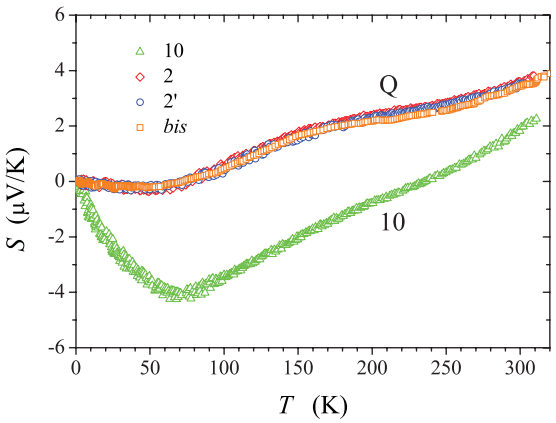

FIG. 8. (Color online) Temperature-dependent thermoelectric power (*S*), measured in the 10, 2, 2′, and *bis* directions. The index Q is conveniently used for the three investigated in-plane directions (2, 2′, and *bis*).

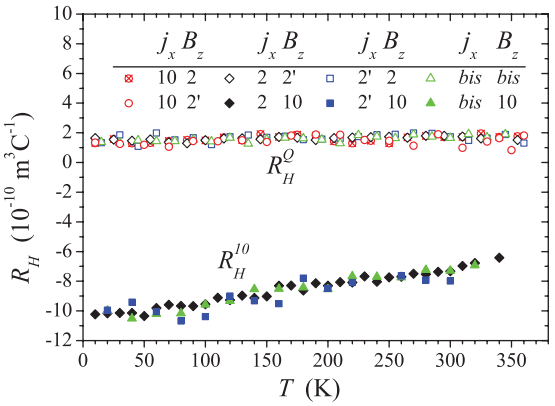

FIG. 9. (Color online) Temperature-dependent Hall coefficient $R_H = E_y/j_x B_z$. Eight sets of experimental data were collected by directing the current j_x along the long axes of the samples, thus in the 10, 2, 2′, and *bis* directions, whereas the magnetic field B_z was directed in the other two orthogonal directions of each sample (details of the current and field directions are given in the legend). The eight R_H data sets form two groups of identical Hall coefficients. The first group (denoted as R_H^Q) contains five data sets, all corresponding to the application of the magnetic field in the quasiperiodic plane, thus in the 2, 2′, and *bis* directions. The second group (denoted as R_H^{10}) contains three sets in which the magnetic field was parallel to the 10-fold direction.

thermopowers (conveniently denoted as S_Q) are positive in most of the investigated temperature range, except at about 40 K, where a minimum with a slightly negative value of -0.2 μV/K is observed.

D. Hall coefficient

The temperature-dependent Hall coefficient $R_H = E_y/j_x B_z$ was determined in the temperature interval between 360 and 10 K. Eight sets of experimental data were collected (Fig. 9) by directing the current j_x along the long axes of the samples, thus in the 10, 2, 2′, and *bis* directions, whereas the magnetic field B_z was directed in the other two orthogonal directions of each sample. The eight R_H data sets form two groups of Hall coefficients with the following regularity. The first group contains five identical data sets, all corresponding to the application of the magnetic field in the quasiperiodic plane, thus in the 2, 2′, and *bis* directions. These data sets show no anisotropy, regardless of the current direction (that was set parallel to the 10, 2, 2′, and *bis* directions) and give a positive holelike and almost temperature-independent value of the Hall coefficient $R_H^Q \approx 1.6 \times 10^{-10}$ m^{3}C^{-1} (where the superscript Q denotes the in-plane direction of the magnetic field) with the experimental uncertainty of $\pm 0.2 \times 10^{-10}$ m^{3}C^{-1}. The second group contains three sets of identical Hall coefficients in which the magnetic field was always parallel to the 10-fold direction, whereas the current was in the three in-plane directions 2, 2′, and *bis*. The application of the field along the 10-fold axis yields a negative electronlike Hall coefficient with the value at 340 K of $R_H^{10} \approx -6.2 \times 10^{-10}$ m^{3}C^{-1} and moderate temperature dependence. The values of both R_H^Q and R_H^{10} are typical metallic. The Hall coefficient thus shows anisotropy, which is related to the direction of the magnetic field and is holelike for the in-plane field application ($R_H^Q > 0$), whereas it changes sign and becomes electronlike ($R_H^{10} < 0$) for the field application along the 10-fold axis. This kind of Hall-coefficient anisotropy is in agreement with the previously published result on d-Al-Co-Ni(Cu) QCs.[24]

E. Specific heat and the electronic density of states at ε_F

Though the specific heat is a scalar quantity and hence does not give information on the anisotropic physical properties of d-Al-Co-Ni, the low-temperature specific heat $C(T)$ is a convenient quantity to estimate the value of the electronic density of states (DOS) at the Fermi energy ε_F and the Debye temperature θ_D. Because our d-Al-Co-Ni material is diamagnetic, the total specific heat is a sum of the electronic and lattice specific heats. The electronic specific heat depends linearly on temperature, $C_{el}(T) = \gamma T$, with the electronic specific heat coefficient $\gamma = (\pi^2/3)k_B^2 g(\varepsilon_F)$, where $g(\varepsilon_F)$ is the DOS at ε_F. At low temperatures below $\sim$10 K, the lattice specific heat can usually be well approximated by the Debye model and is expressed as a function of temperature in the form $C_{\text{latt}}(T) = \alpha T^3$. The lattice specific heat coefficient α is related to the Debye temperature via the relation $\theta_D = (12\pi^4 R/5\alpha)^{1/3}$, where R is the gas constant. The total specific heat at low temperatures can then be written as

$$C(T) = \gamma T + \alpha T^3. \tag{2}$$

The specific heat measurements were performed in the temperature range between 2 and 300 K. The low-temperature molar specific heat is displayed in Fig. 10 in a C/T versus T^2 plot; the specific heat in the entire investigated temperature range is displayed in the inset. The analysis yielded the values $\gamma = 0.52$ mJ/mol·K^2 and $\theta_D = 545$ K. The reference electronic specific heat coefficient of the Al metal is[25] $\gamma_{\text{Al}} = 1.348$ mJ/mol·K^2, which allows estimation of the value of the DOS g at ε_F of d-Al-Co-Ni relative to the Al metal. We obtain $\gamma/\gamma_{\text{Al}} = g/g_{\text{Al}} = 0.39$, so the DOS at ε_F of d-Al-Co-Ni is reduced to 39% of the DOS of the Al metal. The reduced DOS at ε_F is one of the reasons for the moderately high electrical resistivity of d-Al-Co-Ni.

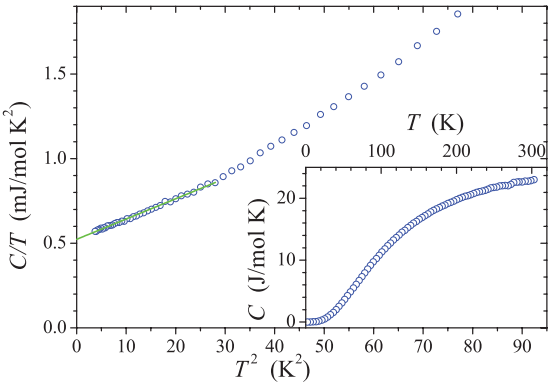

FIG. 10. (Color online) Low-temperature molar specific heat in a C/T versus T^2 plot. The solid line is the fit with Eq. (2). The specific heat in the entire investigated temperature range (2–300 K) is displayed in the inset.

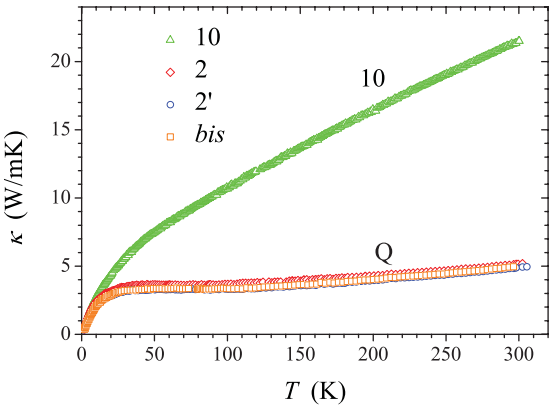

FIG. 11. (Color online) Thermal conductivity κ in the 10, 2, 2′, and *bis* directions. The index Q is conveniently used for the three investigated in-plane directions (2, 2′, and *bis*).

F. Thermal conductivity

The thermal conductivity κ in the 10, 2, 2′, and *bis* directions is displayed in Fig. 11. There is no anisotropy among the three in-plane directions 2, 2′, and *bis* but strong anisotropy to the 10-fold direction, where the thermal conductivity in the 10-fold direction κ_{10} is considerably higher than the in-plane thermal conductivity κ_Q. Both κ_{10} and κ_Q show an initial fast increase at low temperatures up to ∼30 K. Above that temperature, the growth of κ_{10} becomes slower but continues to increase almost linearly up to RT with the 300 K value $\kappa_{10} = 22$ W/mK. In contrast, κ_Q exhibits a plateau above 30 K and grows only insignificantly upon further heating, reaching the RT value of $\kappa_Q = 5$ W/mK.

VI. DISCUSSION

Our measurements of the anisotropic physical properties of a *d*-Al-Co-Ni single crystal in the 10-fold direction and three specific, crystallographically nonequivalent directions within the quasiperiodic plane confirm that a QC of decagonal symmetry is an isotropic solid in the quasiperiodic plane regarding its bulk physical properties, but there exists anisotropy between the quasiperiodic plane and the periodic direction. The theoretical symmetry analysis of a general second-rank tensor that is invariant under the symmetry elements of a decagonal point group is in agreement with the experimental results. In a Cartesian crystal-fixed frame with the z axis in the 10-fold direction and the x and y axes in the 2′ and 2 directions, respectively, the tensor is diagonal and contains only two different diagonal elements, as expressed by Eq. (1), so we determined the complete tensors by specifying the values of a given physical property in the in-plane and the 10-fold directions, e.g., the resistivities ρ_Q and ρ_{10} or the thermopowers S_Q and S_{10}. Though previous studies of the anisotropic physical properties of *d*-QCs did not distinguish among different directions within the quasiperiodic plane (i.e., the measurement direction in the quasiperiodic plane was not specified), the in-plane to the 10-fold direction anisotropy was still correctly determined. However, different degrees of structural perfection of the previously investigated *d*-Al-Co-Ni(Cu) samples of nominally the same composition, and the associated scatter of their physical properties, leave the question about the true intrinsic properties of the *d*-Al-Co-Ni(Cu) phase open, in particular the question about the influence of quasiperiodicity on the physical properties of a solid. For our *d*-Al-Co-Ni material, the high structural quality of the single-crystalline material was confirmed by ^{27}Al NMR symmetry analysis on the local scale of atomic clusters, as well as by structural assessment by other techniques published previously.[18] The high structural quality of our material makes us believe that we are reporting on the true intrinsic physical properties of the *d*-Al-Co-Ni phase. In the following, we discuss the investigated physical properties in view of the preceding open questions.

A. Magnetic properties

The ground state of *d*-Al-Co-Ni is diamagnetic, where the transition metals Co and Ni are in a nonmagnetic state with their *d*-bands fully occupied. Regarding the anisotropy of magnetization and magnetic susceptibility, *d*-Al-Co-Ni QC can be classified as an anisotropic diamagnet with no in-plane anisotropy and moderate anisotropy to the 10-fold direction, which is about two times more diamagnetic direction. Stronger diamagnetism in the 10-fold direction originates from the additional Landau orbital diamagnetic term present for the field application in this direction due to the magnetic force–induced conduction-electron circulation within the decagonal atomic rings located in the quasiperiodic atomic planes. However, the in-plane magnetic susceptibility can be practically fully accounted for by the Larmor diamagnetism of closed atomic core shells. Similar anisotropic magnetism with no in-plane anisotropy and stronger diamagnetism in the stacking (pseudo-10-fold) direction was also found in the Y-phase Al-Co-Ni two-layer decagonal approximant,[10] so long-range quasiperiodicity of the structure plays no role in the (dia)magnetism of *d*-Al-Co-Ni.

B. Electrical resistivity and thermal conductivity

The values of the in-plane and the periodic electrical resistivities and their ratio $\rho_{10}/\rho_Q = 8.4$ of our *d*-Al-Co-Ni are in the range found in previous studies.[3–7] The much larger in-plane resistivity can be attributed to the lack of translational periodicity within the quasiperiodic plane and to the chemical and phason disorder that are at the origin of large residual $T \to 0$ resistivity. Large resistivity in nonperiodic systems is a general effect, also found in, e.g., amorphous metals, so it is not a peculiarity of QCs. The very different temperature dependences of ρ_{10} and ρ_Q can be understood as follows. The periodic ρ_{10} shows temperature dependence typical of regular metals. Away from the low-temperature saturated region, where the plateau in the resistivity is due to elastic electron scattering by quenched defects, the resistivity increases linearly with the temperature and exhibits quite strong PTC, which can be attributed to inelastic electron–phonon scattering. This suggests a ballistic-type motion of conduction electrons in the 10-fold direction (where the mean free path l between scattering events is much larger than the extension of the conduction-electron wave packet L_{wp}) and confirms that phonons are excited in this direction, as expected for a periodic solid. The very weak PTC temperature

dependence of ρ_Q can be, on the other hand, understood in the frame of the theory of slow charge carriers,[26] applicable to systems with weak dispersion of the electronic band energies $E_n(\vec{k})$, where n is the band index and $\vec{k}$ is the wave vector. In such a situation, the electron velocity $\vec{v} = (1/\hbar)\partial E_n(\vec{k})/\partial \vec{k}$ is small, and the traveling distance between two scattering events becomes comparable to the extension of the electronic wave packet ($l \approx L_{\rm wp}$); thus, the motion of electrons is no longer ballistic but becomes diffusive. Moreover, because only long-wavelength acoustic phonons can propagate within the quasiperiodic plane (for which the solid is an elastic continuum), inelastic electron–phonon scattering is largely suppressed and the phonons no longer give the dominant contribution to the temperature dependence of the in-plane resistivity. Weak dispersion of the electronic bands in the Q directions of a model approximant of the d-Al-Cu-Co phase was demonstrated theoretically by Trambly de Laissardière and Fujiwara.[27] The model of slow charge carriers predicts the transition from ballistic to nonballistic electrical conductivity as a function of the relaxation time τ between scattering events that enters the electronic mean free path $l = v\tau$. The electrical conductivity is $\sigma = e^2 g(\varepsilon_F) D$, where D is the electronic diffusion constant that can be written by simple kinetic arguments as $D = v^2\tau/3 = l^2/3\tau$, with v^2 being the mean square electronic speed. For long τ, usually realized at low temperatures, we obtain in the free-electron limit the Drude conductivity $\sigma = ne^2\tau/m$. Because τ shortens with rising temperature, this yields a PTC resistivity in the low-temperature ballistic regime. At higher temperatures, τ becomes short enough to drive the system into the $l \approx L_{\rm wp}$ limit of a nonballistic (diffusive) type of motion. The diffusion constant then becomes inversely proportional to the relaxation time, $D = L^2/\tau$, where L is a constant proportional to the elementary diffusion step. This yields the conductivity of the type $\sigma \propto 1/\tau$ that yields a nonmetallic NTC resistivity in the high-temperature regime.[26] At the transition from the ballistic to the diffusive type of motion, the resistivity exhibits a maximum and a crossover from the low-T PTC to the high-T NTC resistivity. The temperature of the resistivity maximum depends sensitively on the electronic velocity v (hence on the electronic structure and band dispersion), the temperature-dependent relaxation time $\tau(T)$, and the concentration of quenched defects, so different temperature dependences of the resistivity can be obtained for samples of nominally the same chemical composition but different structural perfections and defect concentrations. Various possible temperature-dependent electrical resistivities within the slow-charge-carriers model (PTC, NTC, and mixed PTC-NTC with a maximum), expressed by the formula of the form

$$\rho^{-1} = A\tau + B/\tau, \tag{3}$$

are elaborated on theoretically in detail in our previous publication (see Fig. 7 of Ref. 12). The theory was successfully applied to the complex resistivities of the Al_4(Cr,Fe) decagonal approximant[12] and the giant-unit-cell heavy-fermion intermetallic compound $YbCu_{4.25}$.[28] In Fig. 12(a), we show the fit of the temperature-dependent normalized resistivity $\rho_Q/\rho_{Q,340\,\rm K}$ of our d-Al-Co-Ni from Fig. 7(b) by using Eq. (3). The relaxation time was taken in the form $\tau^{-1} = \tau_0^{-1} + \tau_p^{-1}$, where τ_0^{-1} is the temperature-independent rate due to scattering by

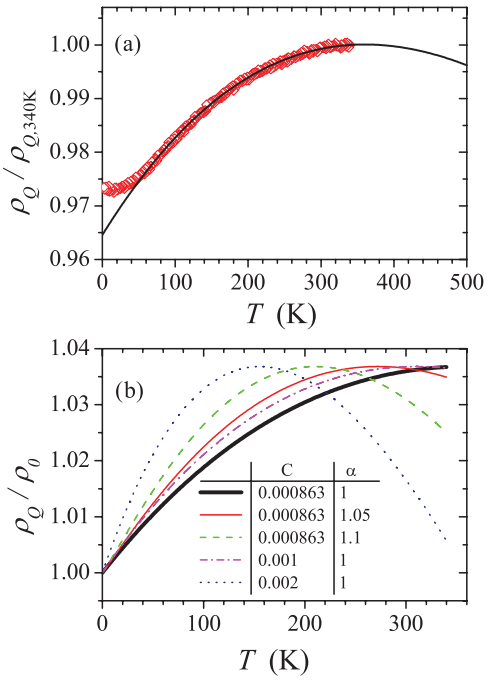

FIG. 12. (Color online) (a) Theoretical fit of the normalized $\rho_Q(T)$ from Fig. 7(b) by using Eq. (4) of the slow-charge-carriers model. The fit parameter values are given in the text. (b) Theoretical $\rho_Q(T)$ curves normalized to the $\rho_0 = \rho(T = 0)$ value for the cases in which the transition from a ballistic to a nonballistic (diffusive) regime would occur at lower temperatures because of stronger disorder in the material (shorter relaxation time τ). The original fit ($C = 8.63 \times 10^{-4}$ and $\alpha = 1.0$) from panel (a) up to the highest temperature of the experimental measurements (340 K) is shown by the bold curve. The modified C and α parameter values of the other curves are given in the legend.

quenched defects, whereas τ_p^{-1} contains any temperature-dependent scattering processes, e.g., scattering by phonons. In the simplest case, τ_p can be phenomenologically written as a power law of temperature $\tau_p = \beta/T^\alpha$, at least within a limited temperature interval. Eq. (3) can then be rewritten in the form

$$\rho^{-1} = \frac{A}{1 + CT^\alpha} + B\,(1 + CT^\alpha), \tag{4}$$

where $A = e^2 g(\varepsilon_F) v^2 \tau_0$, $B = e^2 g\,(\varepsilon_F)\, L^2/\tau_0$, and $C = \tau_0/\beta$. The fit [solid curve in Fig. 12(a)] was made using the parameter values $A = 2.19 \times 10^{-3}$ $(\mu\Omega{\rm cm})^{-1}$, $B = 1.27 \times 10^{-3}$ $(\mu\Omega{\rm cm})^{-1}$, $C = 8.63 \times 10^{-4}$, and $\alpha = 1.0$, where the units of the coefficient C are chosen such that the temperature in the expression CT^α is dimensionless. Eq. (4) reproduces well the temperature-dependent resistivity ρ_Q, except in the low-temperature limit, where it cannot reproduce the $T \to 0$ leveling off. The PTC resistivity with the continuously decreasing slope upon heating is a sign that the conduction-electron system is in the ballistic regime within our investigated temperature range but the temperature-dependent shortening of τ drives the system toward the nonballistic regime, which would be entered at temperatures higher than our highest investigated temperature of 340 K. Extrapolation of the theoretical curve in Fig. 12(a) to higher temperatures indicates that the resistivity maximum would appear at $T = 360$ K.

Eq. (4) allows us to study the effect of shortening τ_p on the shape of the resistivity curve $\rho_Q(T)$ shown in Fig. 12(a), as a consequence of increased dynamic disorder in the lattice. τ_p shortens faster because of either a decrease of the coefficient β [thus increasing the coefficient C in Eq. (4)] or an increased exponent α. Comparing d-Al-Co-Ni samples of nominally the same chemical composition but different structural perfections, τ_p is generally shorter in less perfect samples. Slight increase of the C and α parameter values from those determined in the fit of Fig. 12(a) should thus mimic the resistivity change because of decreased structural perfection. In Fig. 12(b), the original fit from Fig. 12(a) up to the highest temperature of the experimental measurements (340 K) is displayed by the bold curve; the curves with $C = 1 \times 10^{-3}$ and 2×10^{-3} (by keeping the original α value) and the curves with $\alpha = 1$, 1.05, and 1.1 (by keeping the original C value) are shown as well. For all combinations of modified parameters, the transition from PTC to NTC resistivity occurs at lower temperatures, so a slight increase of the disorder either introduces a maximum in the resistivity or changes it from PTC to NTC within the experimentally observed temperature regime.

The preceding result offers the answer to the question about the origin of different literature-reported electrical resistivities in the Q direction of the d-Al-Co-Ni(Cu) QCs of nominally the same composition, where different authors have reported PTC, NTC, or mixed PTC-NTC behavior. The origin of this discrepancy appears to be the different structural perfections of the investigated samples. Structurally more perfect samples generally possess a longer relaxation time τ and hence a longer electronic mean free path $l = v\tau$; thus, the transition from the ballistic PTC to the nonballistic NTC resistivity occurs at higher temperatures, and the PTC resistivity is measured in the temperature range between the $T \to 0$ limit and, e.g., the RT for more perfect samples.

The transport of heat (the thermal conductivity) in d-Al-Co-Ni is in agreement with the transport of the electrical charge (the electrical conductivity). Both are the highest in the 10-fold direction; thus, the d-Al-Co-Ni material is the best electrical and heat carrier in this direction, where both the electrons and the phonons contribute to the transport. Away from the low-temperature $T \to 0$ region, both ρ_{10} and κ_{10} increase with temperature in a linearlike manner that is typical for regular metals and alloys. Within the quasiperiodic plane, the lack of translational periodicity of the lattice largely suppresses the electronic and phononic degrees of freedom, resulting in low values of electrical and thermal conductivity ρ_Q^{-1} and κ_Q and their very weak temperature dependence. The type of anisotropy in ρ and κ observed in d-Al-Co-Ni is not a peculiarity of d-QCs but is a general feature of solids with broken translational periodicity in two dimensions, i.e., a solid with a periodic stacked-layer structure like d-QCs. However, amorphous disorder within the atomic layers is expected to exhibit the same type of anisotropy of electrical and thermal conductivity as the d-QCs.

C. Thermopower and Hall coefficient

Unlike electrical resistivity, which is proportional to the square of the electrical charge ($\rho^{-1} \propto e^2$) and hence does not distinguish between the negative electron-type carriers ($-e$) and the positive hole-type carriers ($+e$), the thermopower S and the Hall coefficient R_H distinguish between the electrons and the holes, because the charge in their expressions appears as e and $1/e$, respectively. S and R_H are thus more sensitive to the details of the anisotropic Fermi surface that is at the origin of the anisotropy of the electronic transport coefficients and the sign reversal of these coefficients for different crystallographic directions. In the absence of a unit cell in the structural description of d-QCs, an *ab initio* calculation of the Fermi surface is not feasible. In our recent work on the Y-phase Al-Co-Ni (Ref. 11) and the orthorhombic $Al_{13}Co_4$ (Ref. 14) decagonal approximants, we showed that the *ab initio* calculated Fermi surfaces change quite drastically for different structural models (one model is usually a refined version of an older model) or even just for the relaxation of an existing model (atoms are shifted by small fractions of interatomic distances to energetically more favorable positions). Thus, conclusions on the electronic transport coefficients of d-QCs on the basis of Fermi surfaces calculated for the approximant phases should be made with great care. Some qualitative conclusions can still be reached on the basis of experimental S_{10}, S_Q, R_H^{10}, and R_H^Q parameters, as shown in Figs. 8 and 9. The in-plane isotropy of S_Q suggests that the Fermi surface of d-Al-Co-Ni is a rotational body around the 10-fold symmetry axis. The rotational symmetry of the Fermi surface was also proposed to be at the origin of the negative electron-type value of R_H^{10} for the field application along the 10-fold axis, as elaborated by Yun-ping *et al.*,[24] whereas the positive hole-type R_H^Q for the in-plane field application was proposed to reflect the Fermi surface curvature typical of nearly full bands in the cross sections perpendicular to the 10-fold symmetry direction. The anisotropies and the temperature dependences of the S_{10}, S_Q, R_H^{10}, and R_H^Q parameters are sensitive to the details of the d-Al-Co-Ni-specific Fermi surface and can be affected by the anisotropic phonon spectrum. In the absence of knowledge of the Fermi surface, a quantitative analysis of the preceding phenomena is not possible. At the qualitative level, the considerably less negative S_Q value at the minimum, as compared to the minimum value of S_{10}, is compatible with the reduced electronic term in the in-plane thermopower, whereas the shift of the S_Q minimum to a lower temperature suggests stronger in-plane phononic/structural scattering than that of the 10-fold direction. Both features correlate reasonably with the much higher in-plane resistivity ρ_Q (and the residual ρ_Q resistivity value at $T = 2$ K), as compared to ρ_{10}.

VII. CONCLUSIONS

We have investigated the anisotropic physical properties of a d-Al-Co-Ni single crystal of exceptional structural quality that was confirmed by both standard materials characterization methods and ^{27}Al NMR spectroscopy on the local scale of atomic clusters. The measurements were performed in the 10-fold (periodic) direction of the structure and in three specific crystallographic directions within the quasiperiodic plane, corresponding to the 2 and 2′ twofold symmetry directions and their bisector. The measurements of the second-rank bulk tensorial properties (the magnetic susceptibility, the electrical

resistivity, the thermopower, and the thermal conductivity) confirm the theoretical prediction that a solid of decagonal point group symmetry should exhibit isotropic physical properties within the quasiperiodic plane and anisotropy between the in-plane and the 10-fold directions. The third-rank Hall-coefficient tensor showed anisotropy related to the direction of the magnetic field, when applied in the 10-fold direction or within the quasiperiodic plane. The electrical and thermal transport is strongly metallic in the periodic crystalline plane but largely suppressed within the quasiperiodic plane, the main reason being the lack of translational periodicity that hinders the propagation of electrons and phonons in a nonperiodic lattice. However, this kind of anisotropy is not a peculiarity of d-QCs but should be a general feature of solids with broken translational periodicity in two dimensions, while retaining the periodicity in the third dimension. For example, any solid with a stacked-layer structure like d-QCs but with amorphous disorder within the atomic layers is expected to exhibit the same type of anisotropy of the electrical and thermal transport coefficients as the d-QCs.

ACKNOWLEDGMENTS

This work was partially supported by the Croatian Ministry of Science, Education and Sports Grant No. 035-0352826-2848.

*jani.dolinsek@ijs.si

[1] A. P. Tsai, A. Inoue, and T. Masumoto, Mater. Trans. **30**, 463 (1989).
[2] T. Gödecke, Z. Metallkd. **88**, 557 (1997).
[3] T. Shibuya, T. Hashimoto, and S. Takeuchi, J. Phys. Soc. Jpn. **59**, 1917 (1990).
[4] J. T. Markert, J. L. Cobb, W. D. Bruton, A. K. Bhatnagar, D. G. Naugle, and A. R. Kortan, J. Appl. Phys. **76**, 6110 (1994).
[5] S. Martin, A. F. Hebard, A. R. Kortan, and F. A. Thiel, Phys. Rev. Lett. **67**, 719 (1991).
[6] W. Yun-ping and Z. Dian-lin, Phys. Rev. B **49**, 13204 (1994).
[7] Q. Guo and S. J. Poon, Phys. Rev. B **54**, 6046 (1996).
[8] Y. Yamada, Y. Yokoyama, K. Matono, K. Fukaura, and H. Sunada, Jpn. J. Appl. Phys. **38**, 52 (1999).
[9] W. Steurer and T. Haibach, in *Physical Properties of Quasicrystals*, edited by Z. M. Stadnik (Springer, Berlin, 1999), pp. 65; P. Gille, G. Meisterernst, and N. Faber, J. Cryst. Growth **275**, 224 (2005).
[10] A. Smontara, I. Smiljanić, J. Ivkov, D. Stanić, O. S. Barišić, Z. Jagličić, P. Gille, M. Komelj, P. Jeglič, M. Bobnar, and J. Dolinšek, Phys. Rev. B **78**, 104204 (2008).
[11] M. Komelj, J. Ivkov, A. Smontara, P. Gille, P. Jeglič, and J. Dolinšek, Solid State Comm. **149**, 515 (2009).
[12] J. Dolinšek, P. Jeglič, M. Komelj, S. Vrtnik, A. Smontara, I. Smiljanić, A. Bilušić, J. Ivkov, D. Stanić, E. S. Zijlstra, B. Bauer, and P. Gille, Phys. Rev. B **76**, 174207 (2007).
[13] J. Dolinšek, S. Vrtnik, A. Smontara, M. Jagodič, Z. Jagličić, B. Bauer, and P. Gille, Phil. Mag. **88**, 2145 (2008).
[14] J. Dolinšek, M. Komelj, P. Jeglič, S. Vrtnik, D. Stanić, P. Popčević, J. Ivkov, A. Smontara, Z. Jagličić, P. Gille, and Y. Grin, Phys. Rev. B **79**, 184201 (2009).
[15] P. Popčević, A. Smontara, J. Ivkov, M. Wencka, M. Komelj, P. Jeglič, S. Vrtnik, M. Bobnar, Z. Jagličić, B. Bauer, P. Gille, H. Borrmann, U. Burkhardt, Y. Grin, and J. Dolinšek, Phys. Rev. B **81**, 184203 (2010).
[16] M. Heggen, M. Feuerbacher, J. Ivkov, P. Popčević, I. Batistić, A. Smontara, M. Jagodič, Z. Jagličić, J. Janovec, M. Wencka, and J. Dolinšek, Phys. Rev. B **81**, 184204 (2010).
[17] W. Steurer and A. Cervellino, Acta Crystallogr. A **57**, 333 (2001).
[18] B. Bauer, G. Meisterernst, J. Härtwig, T. Schenk, and P. Gille, Philos. Mag. **86**, 317 (2006).
[19] P. Jeglič, M. Komelj, M. Klanjšek, U. Tkalec, S. Vrtnik, M. Feuerbacher, and J. Dolinšek, Phys. Rev. B **75**, 014202 (2007).
[20] P. Jeglič and J. Dolinšek, Phys. Rev. B **71**, 014204 (2005).
[21] P. W. Selwood, *Magnetochemistry* (Interscience Publishers, New York, 1956).
[22] S. E. Burkov, Phys. Rev. Lett. **67**, 614 (1991).
[23] W. Steurer and K. H. Kuo, Acta Crystallogr. B **46**, 703 (1990).
[24] W. Yun-ping, Z. Dian-lin, and L. F. Chen, Phys. Rev. B **48**, 10542 (1993).
[25] U. Mizutani, *Introduction to the Electron Theory of Metals* (Cambridge University Press, Cambridge, 2001), pp. 43.
[26] G. Trambly de Laissardière, J.-P. Julien, and D. Mayou, Phys. Rev. Lett. **97**, 026601 (2006).
[27] G. Trambly de Laissardière, and T. Fujiwara, Phys. Rev. B **50**, 9843 (1994).
[28] J. Dolinšek, M. Wencka, M. Jagodič, Z. Jagličić, S. Gottlieb-Schönmeyer, F. Ritter, and W. Assmus, Solid State Comm. **150**, 1629 (2010).